Title

Models of the putative antimony(v)–diolate motifs in antileishmanial pentavalent antimonial drugs

Journal

Dalton Transactions, 52(27)

ISSN

1477-9226

Authors

Lindquist-Kleissler, Brent
Johnstone, Timothy C

Publication Date

2023-07-11

DOI

10.1039/d3dt01623d

Models of the putative antimony(V)-diolate motifs in antileishmanial pentavalent antimonial drugs

*Brent Lindquist-Kleissler and Timothy C. Johnstone**

Department of Chemistry and Biochemistry, University of California Santa Cruz, Santa Cruz, California 95064, United States.

* Correspondence to: johnstone@ucsc.edu

Abstract

The structures of the pentavalent antimonials, small-molecule Sb-containing drugs used to treat the neglected tropical disease leishmaniasis, remain unknown despite their widespread use for over half a century. These drugs are prepared by combination of an Sb(V) precursor and a sugar derivative and proposed structures frequently invoke a cyclic stiborane motif in which a vicinal diolate ligand chelates an Sb(V) center. As a step towards better understanding the structures of the pentavalent antimonial drugs, a series of cyclic organostiboranes spanning the stereochemical space afforded by a vicinal diolate motif has been synthesized and characterized. X-ray crystallography and NMR spectroscopy provide unambiguous characterization of the structures of these model compounds and of the interaction of the diolate with the Sb(V) center. Particularly notable are the systematic trends observed in the NMR spectroscopic signals as a function of the stereochemistry of the diolate. The spectroscopic signatures identified with these model compounds will provide a framework for elucidating the structures of the pentavalent antimonial drugs.

Introduction

Despite – or perhaps because of – the high toxicity of many Sb-containing molecules, this class of compounds has a rich history in therapeutic medicine.[1] One of the oldest reported Sb-containing therapeutics of defined molecular composition is the potassium salt of the tartrate complex of Sb(III), typically called potassium antimony tartrate or tartar emetic.[2] As the latter name implies, the compound was widely used to induce vomiting, and interestingly is still used for this purpose in ornithological studies.[3] Although used medicinally for over 300 years, the structure of this molecule was not confirmed until the 1960s, when a variety of studies revealed that it featured two four-coordinate Sb centers, each with a square-based pyramidal geometry.[4] This example serves to highlight the difficulty that can attend the elucidation of the structures of Sb-containing drugs, although the information was not used to improve Sb-based emetics because their clinical use had largely ended by that time. Sb-containing therapeutics are still used, however, to treat the neglected tropical disease leishmaniasis.[5] Up to a million new cases of leishmaniasis are reported annually, mostly in low- and middle-income countries.[6] The Sb-containing antileishmanial drugs meglumine antimoniate (Glucantime) and sodium stibogluconate (Pentostam) are collectively known as the pentavalent antimonials. Although the pentavalent antimonials have remained some of the most effective treatments for leishmaniasis for nearly a century, they have many serious side effects that reduce patient quality of life; antimonial therapy can even be fatal.[7] Attempts to rationally capitalize on their antileishmanial activity while reducing off-target toxicity are hampered by the fact that, as was once the case with potassium antimony tartrate, there is little-to-no information on the structures of these molecules. Unlike potassium antimony tartrate, however, the pentavalent antimonials are still in

widespread clinical use and knowing their structures could provide a framework for rationally developing more active or selective derivatives and understanding their mechanism of action. This information would also be invaluable in addressing one of the larger questions concerning the pentavalent antimonials: is each drug (i) an intractable mixture of multiple compounds or (ii) a set of one or more well-defined compounds with other species present as minor components? If any mixture of molecules is present in these drugs, it may be the case that the components have differential toxicity and activity. Both drugs are synthesized by combining an Sb(V) precursor and a polyalcohol, either *N*-methyl-D-glucamine or D-gluconic acid.[8] The oxophilicity of Sb(V) suggests that Sb binds to the polyalcohol ligand through one or more deprotonated hydroxyl groups, and their arrangement on the ligand backbone makes it likely that the Sb centers are chelated by at least two of these groups (Scheme 1). Chelation via vicinal alkoxide groups is particularly favorable because it permits the formation of unstrained five-membered rings. A large variety of different structures has been proposed for the pentavalent antimonials, many of which are informed by mass spectrometry studies.[8] Despite the value of the information provided by these measurements, they do not discriminate readily among the myriad of ways that these sugar derivatives can interact with the metalloid.[9] Mass spectrometric analysis is also complicated by the possibility that the dative Sb–O bonds are sufficiently labile to rearrange during ionization.

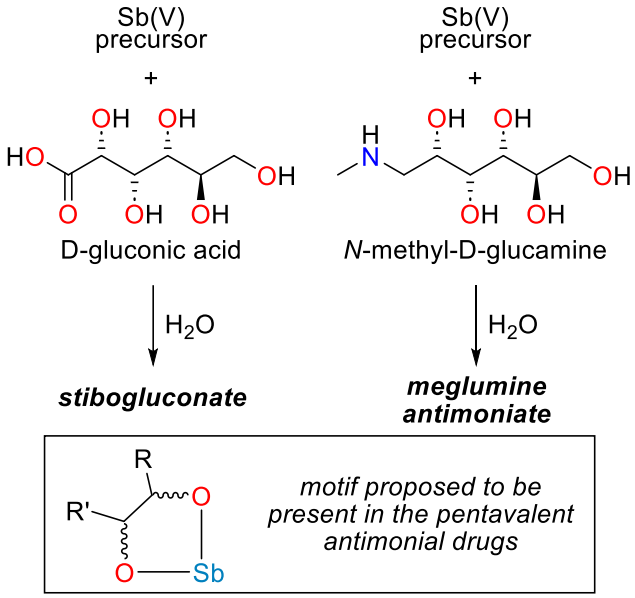

Scheme 1. Overall synthesis of the antileishmanial pentavalent antimonial drugs stibogluconate and meglumine antimoniate from an Sb(V) precursor such as hydrolyzed $SbCl_5$ or $K[Sb(OH)_6]$. Boxed at bottom is a representation of the chelating diolate motif commonly proposed to be present in the drugs.

Gaining insight into the structures of these drugs with direct spectroscopic studies is hampered by the lack of distinct spectroscopic signatures corresponding to the different possible binding modes of the ligands. To provide a foundation for such studies, we have targeted the synthesis of model compounds featuring well-characterized instances of an Sb(V) center chelated by a vicinal diolate. We note that in the case of D-gluconic acid, the carboxylate could also bind to the Sb center, but in the present work we have restricted our investigation to the vicinal diolate motif. In the case of both *N*-methyl-D-glucamine and D-gluconic acid, there are three types of vicinal hydroxyls to which the Sb can bind: those with the same stereochemistry (i.e., *R*,*R*), those with opposite stereochemistry (i.e. *R*,*S*), and one secondary alcohol and one primary alcohol (Scheme 2).

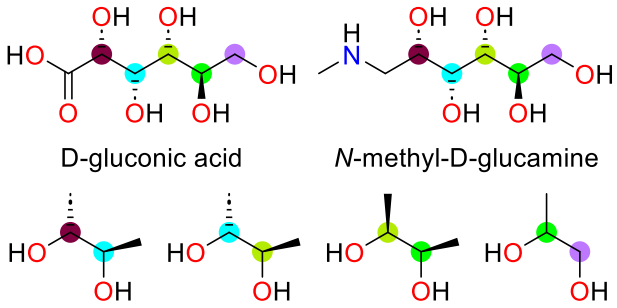

Scheme 2. Depiction of the relationship between the stereochemistry of the vicinal diols used in this study (*bottom*) and the stereochemistry of the *N*-methyl-D-glucamine and D-gluconic acid ligand precursors used in the pentavalent antimonial antileishmanial drugs (*top*).

Based on our previous work,[10] we chose to use the $Sb(tol)_3$ fragment as the framework upon which to install the chelating diolate. The advantages of this organometallic framework include its stability, ease of synthesis, and solubility in a variety of solvents. The stibine $Sb(tol)_3$ was oxidized and then converted into one of a series of six cyclic organostiboranes (Scheme 3). We have selected a set of simple diols that recapitulate the motifs from Schemes 1 and 2. We report here the synthesis and characterization of these model compounds, including X-ray crystal structure determinations. Analysis of their NMR spectra revealed that each of the three binding modes exhibits a distinct spectroscopic signature. This information will be useful in understanding the interactions of the more complex sugar-derived ligands present in the antimonial antileishmanial drugs meglumine antimoniate and sodium stibogluconate.

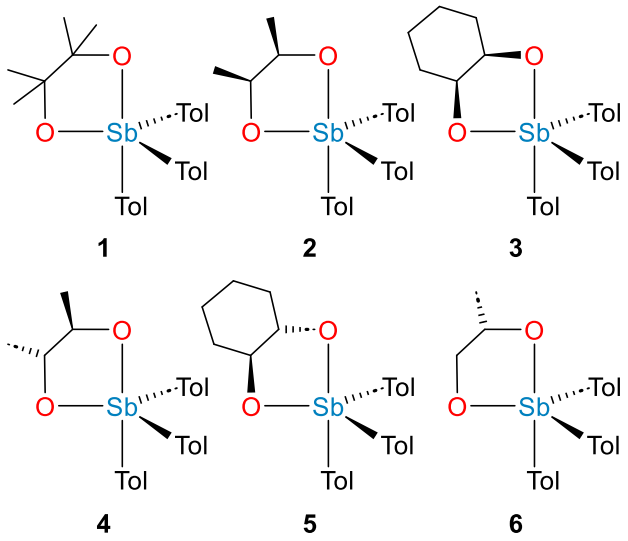

Scheme 3. Structures of model compounds **1**-**6** investigated in this study.

Results and Discussion

Synthesis

Although we will discuss **1**-**6** as Sb(V) complexes bearing chelating diolate ligands, it should be borne in mind that they can alternatively be viewed as derivatives of the five-membered 1,3-dioxa-2-stibolane heterocycle in which the coordination number (σ) and valence (λ) of the Sb center are both increased to five. The majority of 1,3-dioxa-2-(σ^5,λ^5)-stibolanes reported in the literature correspond to Sb(V) centers bearing chelating dicarboxylates or α-hydroxycarboxylates.[11-13] There are, however, examples in which the chelating diolate motif is used and an analog of **1** (with Ph instead of tol substituents) has been previously reported.[14] The isolation of this analog of **1** was achieved by insertion of $SbPh_3$ into the O–O bond of 3,3,4,4-tetramethyl-1,2-dioxetane, which can alternatively be described as oxidative addition of the 1,2-dioxetane derivative to the stibine.[14] A compound similar to **6** but featuring a 1,2-ethanediolate ligand instead of a 1,2-propanediolate ligand, was prepared by oxidizing a triarylstibine with *tert*-butyl hydroperoxide in the presence of ethylene glycol.[15] An analog of **1** in which the Sb

center bears one tolyl group and is chelated by two pinacolate ligands was prepared from tolylstibonic acid.[16] Finally, we note that 1-oxa-3-aza-2-(σ^5,λ^5)-stibolanes have been prepared from dihalostiboranes and *o*-aminophenols in a manner similar to that which we will describe below.[17]

Compounds **1**-**6** were synthesized via the route depicted in Scheme 4. An equimolar mixture of $Sb(tol)_3Br_2$ and a diol were stirred at room temperature in DCM with 2 equiv Et_3N for 1 h. The solvent was removed to yield a mixture of the target compound and $(Et_3NH)Br$. The Sb(V) compound was extracted with Et_2O and recrystallized from MeCN at –20 °C to yield colorless crystals. Alternatively, the solid mixture of the target compound and $(Et_3NH)Br$ could be washed with H_2O to remove the $(Et_3NH)Br$ and leave the product, but this procedure appeared to promote hydrolysis of the target compounds, resulting in complex mixtures containing oxo-bridged species, including the oxo-bridged species $[(tol)_3Sb(\mu\text{-}C_4H_8O_2)]_2O$, which was crystallographically characterized (Figure S1). The synthesis of 1-oxa-3-aza-2-(σ^5,λ^5)-stibolanes noted above similarly involved the combination of a dihalostiborane, the ligand to be installed, and a non-nucleophilic base. That work was performed in toluene and although we have confirmed that our chemistry does proceed in that solvent as well, we obtained cleaner products from DCM.

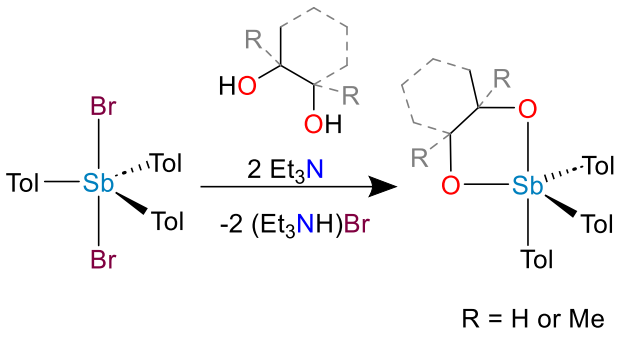

Scheme 4. Synthesis of **1**-**6**.

The synthesis of **1** served to validate our synthetic methodology and to provide a foundation for our analyses by using the pinacolate ligand that lacks stereocenters. Compound **4**, prepared with 2*R*,3*R*-butanediol, provides an example of a complex featuring a chelating diolate with stereocenters of identical handedness. Compound **5**, prepared with 1*S*,2*S*-cyclohexanediol, allowed us to explore whether changing the diolate ligand while preserving the relative handedness of the stereocenters would impact the product. The syntheses of **2** and **3**, prepared from the *meso* compounds 2*R*,3*S*-butanediol and 1*R*,2*S*-cyclohexanediol respectively, were similarly motivated. These latter two species allowed us to investigate the chelation by vicinal diolates in which the ligand stereocenters have opposite handedness. Finally, **6**, prepared from *S*-1,2-propanediol, provides a means of modelling coordination by a vicinal diolate featuring one primary alkoxide and one secondary alkoxide.

X-ray crystallography

The identities of all six compounds were unambiguously confirmed crystallographically (Figure 1 and Table 1). The starting stibine $Sb(tol)_3$ was also crystallographically characterized (see ESI and Figure S2). Crystals of **1**-**6** suitable for X-ray diffraction analysis were grown from saturated MeCN solutions at –20 °C for all compounds. Compound **1**, lacking any stereogenic C centers, unsurprisingly crystallized in the centrosymmetric space group $P2_1/c$. The diols used to prepare **2** and **3** are *meso* compounds and these Sb(V) complexes also crystallized with centrosymmetry, both crystal structures belonging to space group $P\bar{1}$. Compounds **4**-**6** were prepared using enantiomerically pure diols and, as expected, crystallized in Sohncke space groups. Crystals of **4**, **5**, and **6** all feature two molecules in the asymmetric unit and in each case the two molecules are related by a pseudoinversion center. For all three crystal structures, the

pseudosymmetry is observed by the Sb atom and aryl rings, but not by the enantiomerically pure diolate ligand. In the case of **4** (Figure 2), the pseudoinversion center lies at (0.74, 0.50, 0.76); a true inversion center at (0.75, 0.50, 0.75) would afford space group C_2/c. In the case of **5**, the pseudoinversion center lies at (0.49, 0.48, 0.50) and a true inversion center at (0.50, 0.50, 0.50) would afford space group $P\bar{1}$. In the case of **6**, the pseudoinversion center lies at (0.75, 0.75, 0.25); a true inversion center at this location would afford space group *Pbca*. The Flack parameters for **4**, **5**, and **6** do not deviate from 0 within 3σ, consistent with our proposal that these pseudoinversion centers are not missed true crystallographic symmetries.

Table 1. Refinement details for the crystal structures of compounds **1**-**6**.

	1	**2**	**3**	**4**	**5**	**6**
Formula	$C_{27}H_{33}O_2Sb$	$C_{25}H_{29}O_2Sb$	$C_{27}H_{31}O_2Sb$	$C_{25}H_{29}O_2Sb$	$C_{27}H_{31}O_2Sb$	$C_{24}H_{27}O_2Sb$
FW	511.28	483.23	509.27	483.23	509.27	469.20
T (K)	100(2)	101(1)	101(2)	100.5(9)	100(1)	100(1)
λ (Å)	1.54184	1.54184	1.54184	1.54184	1.54184	1.54184
Crystal System	Monoclinic	Triclinic	Triclinic	Monoclinic	Triclinic	Orthorhombic
Space group	$P2_1/c$	$P\bar{1}$	$P\bar{1}$	$C2$	$P1$	$P2_12_12_1$
a (Å)	9.82520(10)	8.6242(2)	10.0944(4)	13.81140(10)	8.8969(2)	15.1979(5)
b (Å)	11.8813(2)	9.3045(2)	11.6974(5)	11.47050(10)	9.3354(2)	16.3230(8)
c (Å)	20.2807(3)	14.1213(3)	12.2709(6)	28.9055(2)	15.1475(4)	16.9475(6)
α (°)		79.804(2)	63.873(5)		76.082(2)	
β (°)	90.7870(10)	83.183(2)	84.156(4)	103.8970(10)	78.930(2)	
γ (°)		80.822(2)	65.488(4)		74.721(2)	
Volume (Å^3)	2367.27(6)	1096.19(4)	1177.82(11)	4445.27(6)	1166.83(5)	4204.3(3)
Z	4	2	2	8	2	8
ρ_{calc} (Mg/m^3)	1.435	1.464	1.436	1.444	1.449	1.483
Size (mm^3)	0.16×0.09× 0.06	0.15×0.13× 0.06	0.11×0.07×0.04	0.18×0.10×0.07	0.11×0.08×0.06	0.09×0.06×0.05
θ range (°)	4.313-67.684	3.194-67.684	4.032-67.070	3.150-67.684	3.034-66.575	3.760-67.684
Total data	33440	27604	27689	68817	28265	60946
Unique data	4482	4461	4184	8124	7799	7984
Parameters	278	258	338	516	585	496
Completeness	100.0%	99.7%	99.7%	99.9%	100.0%	100.0%
R_{int}	5.16%	7.09%	6.63%	4.92%	4.56%	9.96%

R_1 (I > 2σ)	2.37%	3.10%	3.92%	2.04%	2.51%	4.83%
R_1 (all data)	2.61%	3.21%	4.38%	2.05%	2.63%	5.71%
wR_2 (I > 2σ)	6.14%	8.17%	9.39%	5.31%	6.05%	11.56%
wR_2 (all data)	6.28%	8.25%	9.61%	5.31%	6.12%	11.99%
S	1.050	1.101	1.093	1.031	1.047	1.080
Flack x	—	—	—	-0.009(5)	-0.021(10)	0.001(13)

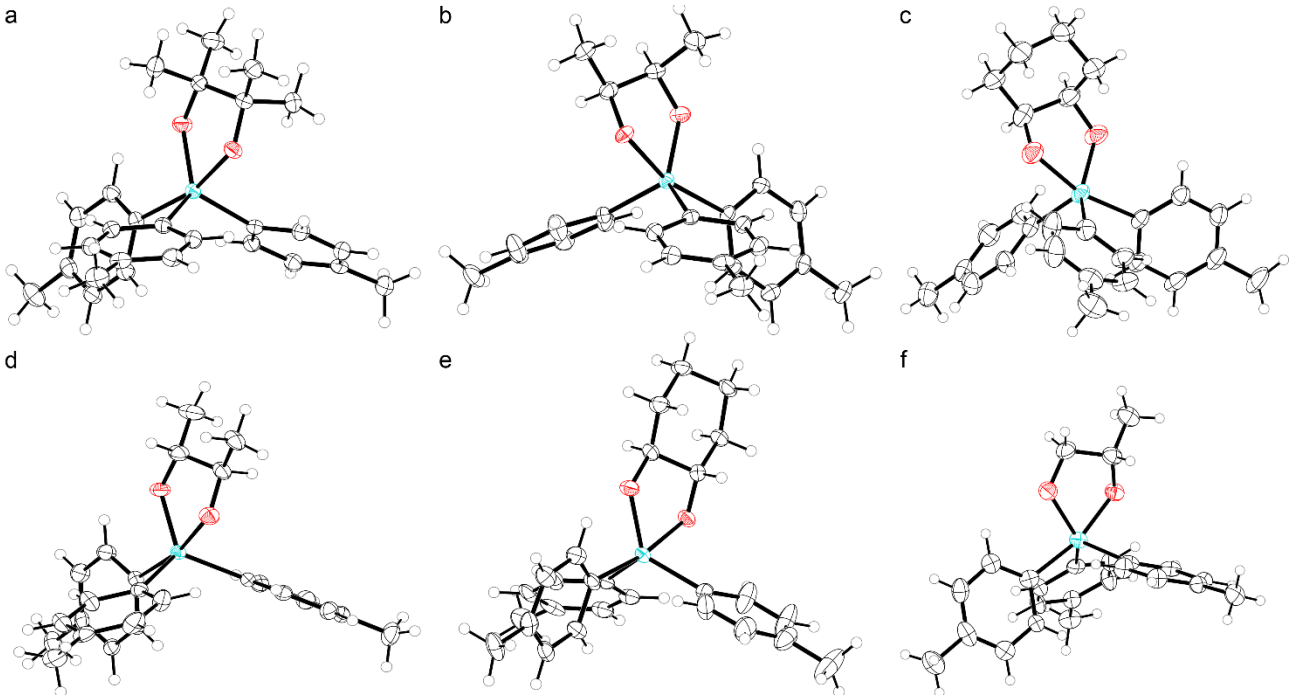

Figure 1. Thermal ellipsoid plots (50% probability) of **1**-**6** (a-f). Color code: Sb teal, O red, C black, H white spheres of arbitrary radius. For crystals with $Z' > 1$ (d-f), only one of the molecules in the asymmetric unit is shown. For **3** (c), only the major component of the disorder is shown.

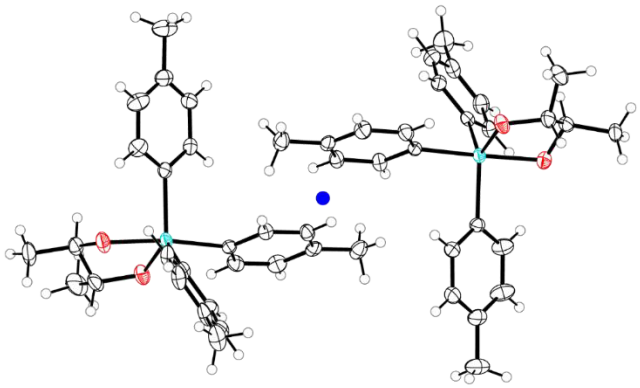

Figure 2. Thermal ellipsoid plot (50% probability, H atoms as spheres of arbitrary radius) of the complete asymmetric unit of the crystal structure of **4.** Blue disc represents the pseudoinversion center between the two molecules. Color code: Sb teal, O red, C black, H white.

Geometry

The structure of each of the 2,3-butanediolate complexes superimposes upon that of its corresponding 1,2-cyclohexanediolate counterpart (**2** upon **3**; **4** upon **5**) (Figures S3a and S3b). Because **4** was prepared from 2*R*,3*R*-butanediol and **5** was prepared from 1*S*,2*S*-cyclohexanediol, their direct comparison requires inversion. The 2*R*,3*R*-butanediolate (**4**) and 1,2-propanediolate (**6**) complexes superimpose upon the pinacolate complex (**1**) with successively more H atoms replaced by methyl groups (Figure S3c). These comparisons suggest that the molecular geometries obtained in these crystallographic experiments do indeed reflect the lowest-energy structures of these molecules. The difference in the backbone stereochemistry for **3** and **5** also results in the cyclohexyl ring of **3** deviating significantly from coplanarity with the SbO_2C_2 ring (Figure 3a); the angles between the normals of the planes that best fit the SbO_2C_2 ring and the C_6 ring for the two components of the disorder are 121.2(3)° and 121.4(5)°. In contrast, the corresponding angles for the two crystallographically inequivalent molecules in the structure of **5**

are 1.2(3)° and 2.1(3)°. Valence-shell electron pair repulsion (VSEPR) theory predicts that the most stable geometry for pentasubstituted, pentavalent (σ^5, λ^5) metal/metalloid compounds is trigonal bipyramidal (D_{3h}). The square pyramidal (C_{4v}) geometry is the other most commonly encountered for this coordination number. The τ parameter is useful in describing the geometry of such molecules because it captures the position of the molecule along the C_{2v}-symmetric normal coordinate that connects C_{4v} square pyramidal (τ = 0) and D_{3h} trigonal bipyramidal (τ = 1) geometries.[18] Interestingly, **1**-**6** display a large range in τ values, from 0.33 for **3** to 0.82 for **5** (Figure 3b). The two compounds prepared from the *R*,*S*-diols (**2** and **3**) had the lowest τ values, and those prepared from the *R*,*R*- or *S*,*S*-diols (**4** and **5**) had the highest τ values (Table 2).

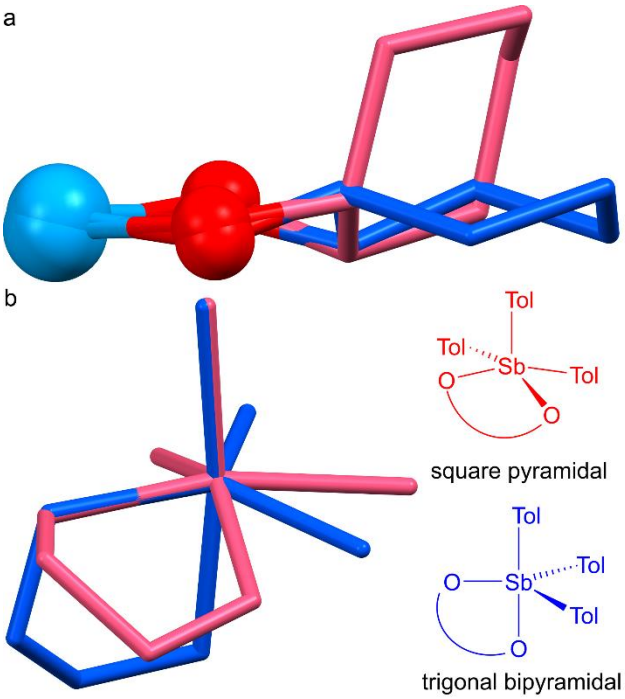

Figure 3. a) Side view of an overlay of the Sb-diolate moieties of **3** (light red) and **5** (blue) shown as sticks with the Sb and O atoms shown as teal and red spheres, respectively. b) Overlaid stick diagrams of square pyramidal **3** (light red, τ = 0.33) and trigonal bipyramidal **5** (blue, τ = 0.82) showing the differences in geometry about the Sb center. Tolyl groups are omitted for clarity.

Table 2. Crystallographically determined bond metrics for **1**-**6**.

	τ[c]	Sb–O (Å)
1	0.56	1.9802(15), 2.0182(16)
2	0.45	1.990(2), 2.0211(19)
3[a]	0.33	1.986(8)/2.018(5), 2.017(3)
4[b]	0.75	1.975(3), 2.023(3) / 1.979(3), 2.023(3)
5[b]	0.82	1.981(6), 2.042(6) / 1.978(6), 2.045(6)
6[b]	0.64	1.980(7), 2.055(6) / 1.976(7), 2.050(6)

[a] Sb–O values provided for both components of the disordered cyclohexanediolate.
[b] Sb–O values provided for both crystallographically independent molecules in the asymmetric unit.
[c] Average values provided in instances of disorder or multiple crystallographically independent molecules.

Conformational isomers

These molecules all feature five-membered chelate rings containing the Sb atom, the O atoms, and the two backbone C atoms. The puckering of this nonplanar 1,3-dioxa-2-stibolane ring can be described using the ring twist notation with chirality assigned as either λ or δ using the skew lines convention. For the achiral diolate ligands, the two conformations are isoenergetic; both are present in the crystal structures of **1**, **2**, and **3**. The major component of the disorder for **3** features the cyclohexane puckered in such a fashion as to afford the δ ring twist conformation of the chelate ring. The minor component of the disorder features the flipped chair conformation of the cyclohexane unit, giving rise to the λ ring twist conformation of the chelate ring. The centrosymmetry of the space group of the crystal structure of **3** ($P\bar{1}$) ensures that both ring twist conformations are present in equal proportions. In contrast, the structures of **4** and **5** feature only one ring twist isomer each: **4**, prepared from the *R*,*R* butanediol, crystallized as the λ isomer and **5**, prepared from the *S*,*S* cyclohexanediol, crystallized as the δ isomer (Figure 4). The puckering isomers observed for **4** and **5** are those which allow the methyl groups to assume the

less sterically encumbered equatorial positions on the puckered ring. In the case of **6**, the δ isomer that is observed crystallographically is again that which allows the methyl bound to C2 of the 1,2-propanediolate to assume an equatorial position on the five-membered ring. Finally, we note that only the *R*,*R* or *S*,*S* substitution patterns allow both vicinal substituents on the five-membered ring to assume equatorial positions. For **2** and **3**, which were prepared from *R*,*S* diols, one substituent is necessarily equatorial and the other is axial. Although these structural data indicate that the chiral diols afford a thermodynamic preference for a specific conformational isomer, the barrier to interconversion between these λ or δ isomers can be low and they most likely interconvert in solution.

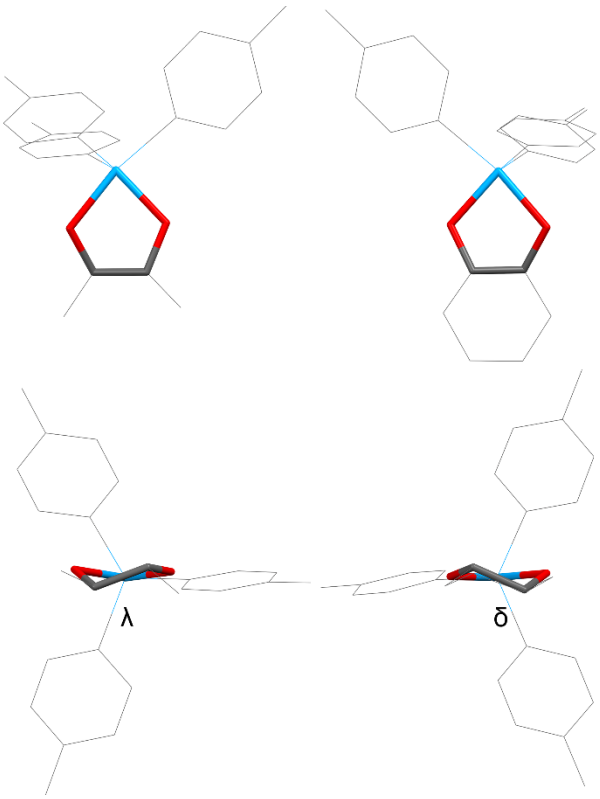

Figure 4. Crystallographically determined molecular structures of **4** (*left*) and **5** (*right*) shown with the five-membered chelate ring parallel (*top*) and perpendicular (*bottom*) to the page. The

labels indicate the different ring conformations. The atoms forming the chelate ring are shown as sticks and all others as lines. Hydrogen atoms omitted for clarity. Color code: Sb teal, O red, C grey.

The molecules possess Sb–O bond lengths ranging from 1.975(3) Å for **4** to 2.055(6) Å for **6** (Table 2). For all compounds, there is one shorter Sb–O bond of approximately 1.98 Å and a slightly, but statistically significantly, longer one that is 2.02-2.05 Å in length. The longest of the shorter Sb–O bond lengths, and the smallest discrepancy between the short and long, was observed for the compounds prepared from the *R*,*S* diols (**2** and **3**). It is notable that these are the two compounds that also deviate most strongly from trigonal bipyramidal toward square pyramidal (Table 2). In the case of the trigonal bipyramidal compounds, the longer Sb–O bond is consistently identifiable as the axial, whereas the shorter is the equatorial, as expected given the three-center-four-electron bonding expected along the trigonal bipyramidal axis.

NMR spectroscopy

Although the diols used to prepare **1**-**5** all have internal symmetries, the crystallographically determined structures described above highlight that binding to the $Sb(tol)_3$ moiety, particularly when forming trigonal bipyramidal complexes, results in a desymmetrization of the diolate. Such a lowering of symmetry would be expected to manifest in the NMR spectra of these compounds if not for the fact that pentasubstituted pnictogen molecules are frequently highly fluxional.[10,19,20]

For example, under the assumption that **1**, **2**, and **4** are trigonal bipyramidal in solution, one would expect to see two distinct methyl resonances in the ^{1}H NMR spectrum of each: one

for the methyl group(s) closest to the O atom that is bound axially, and one for the methyl group(s) closest to the O atom bound equatorially. For **2** and **4**, these methyl peaks should be further split by the backbone CH units into doublets. Instead, the ^{1}H NMR spectra of **2** and **4** each feature a single doublet integrating to 6H (all NMR spectroscopic studies were performed in $CDCl_3$). The spectrum of **1** similarly features a single ^{1}H methyl resonance and all three compounds feature a single methyl resonance in their ^{13}C NMR spectrum. These data clearly confirm that these molecules are fluxional on the NMR time scale, and that some form of polytopal rearrangement (likely related to the Berry pseudorotation) allows the methyl groups to exchange chemical environments. The spectra of the 1,2-cyclohexanediolate complexes **3** and **5** are similarly devoid of the complexity expected for non-fluxional species. The unsymmetrical diolate ligand in **6** would exhibit the same number of NMR signals whether or not it was fluxional. We have not been able to observe low-temperature decoalescence of any of the NMR signals for **1**-**6**.

With these six model compounds in hand, we assessed whether NMR spectroscopy would provide signatures for the different types of metalloid-ligand interactions (Scheme 2). We first analyzed the change in the ^{13}C resonances of the C atoms bound directly to the coordinating O atoms. For the pinacolate-containing **1**, there is an upfield shift for this resonance, as compared to the corresponding resonance of pinacol. A similar upfield shift is observed for both of the Sb compounds derived from *R*,*S* diols (**2** and **3**). In contrast, the compounds derived from the *R*,*R*/*S*,*S* diols exhibited either a smaller upfield shift (**4**) or a marked downfield shift (**5**). We observed a similar distinction between **2**/**3** and **4**/**5** in the ^{1}H NMR resonances of the OC*H* nuclei of the diols and bound diolates (Figure S4). For **2** and **3**, the OC*H* resonance shifts downfield

upon binding to the Sb(V) center (Table 3). In contrast, there is a upfield shift in the OC*H* resonance for both **4** and **5** (Table 3).

Table 3. NMR spectroscopic signatures in $CDCl_3$ of metalloid-ligand interactions in **1**-**6**.[a]

	$\Delta(\delta^{13}C_{OC})$	$\Delta(\delta^{1}H_{OCH})$
1	–1.45	–
2	–2.27	+0.13
3	–1.50	+0.03
4	–0.28	–0.04
5	+1.62	–0.22
6 (CH)	–2.75	+0.03
6 (CH_2)	–0.72	+0.36, –0.19

[a] Changes in δ were calculated by subtracting the value of the bound ligand from that of the free diol.

Compound **6**, prepared from *S*-1,2-propanediol, provides an interesting comparator for **1**-**5**. Because the chelating ligand in **6** binds to the Sb center through one primary alkoxide and one secondary alkoxide, there are two distinct ^{13}C NMR signals and three distinct ^{1}H signals from the chelate ring (the OCH_2 unit exhibits diastereotopic splitting). Both ^{13}C resonances are shifted upfield in the Sb complex, but the O*C*H unit shifts by significantly more. The ^{1}H shifts are more variable with the OC*H* signal shifting slightly downfield, while one of the OCH_2 signals shifts strongly upfield and the other shifts strongly downfield. The most significant advantage gained by the desymmetrization of the ligand, however, is that all of the coupling constants between the ligand proton resonances can be obtained from a first-order spectral analysis (Figure S5). Upon binding to Sb(V), the $^{3}J_{HH}$ value for the coupling of the OC*H* to one of the OCH_2 protons increases by 2 Hz whereas that for coupling to the other OCH_2 proton decreases by 0.4 Hz. These shifts are fully consistent with those expected upon transitioning from a staggered antiperiplanar configuration in the free diol to a staggered gauche configuration in the complex (Figure S5). The slight decrease of 0.4 Hz for one of the OCH_2 protons even suggests that the

gauche configuration is not perfectly staggered and that the H–C–C–H dihedral angle for this interaction is slightly less than 60°. Indeed, analysis of the crystal structure of **6** affords H–C–C–H dihedral angles for this H atom of 49.5(9)° and 43.2(9)° for the two crystallographically independent molecules in the asymmetric unit.

Conclusion

The pentavalent antimonial drugs remain an important last line of defence against leishmaniasis, but important issues of toxicity and rising levels of Sb resistance in the causative parasites motivate further research into the fundamental chemistry and biology of these drugs. Notably, however, the stark lack of information about their molecular structures greatly inhibits the community's ability to understand and rationally improve the safety/activity of these drugs. The polyalcohol structure of the carrier ligands used in the preparation of the pentavalent antimonial drugs suggests that chelating polyalkoxide motifs are likely present. Here, we have prepared small molecule models of Sb(V) complexes for each of the distinct classes of vicinal diolate environments possible in sodium stibogluconate and meglumine antimoniate. All of the motifs can indeed form stable chelate complexes, which allowed us to establish the spectroscopic signatures of each. Perhaps most diagnostic is the variation in the $^{3}J_{HH}$ values following Sb binding of a primary-secondary diol. We will continue to collect further spectroscopic signatures to ultimately extract meaningful structural information from the NMR spectra of the pentavalent antimonial drugs.

Experimental Methods

General methods. All solvents and reagents were commercially available and used as received unless stated otherwise. $Sb(tol)_3$ and $Sb(tol)_3Br_2$ were prepared as previously described.[21,22] Et_2O was dried using 3-Å molecular sieves. $CDCl_3$ was purchased from Cambridge Isotope Laboratories and used as received. ^1H and $^{13}C\{^1H\}$ NMR spectra were recorded on a Bruker Avance III HD 500 MHz NMR spectrometer equipped with a multinuclear Smart Probe. Chemical shifts in the ^1H and $^{13}C\{^1H\}$ NMR spectra are reported in ppm as chemical shifts from tetramethylsilane and were referenced using the $CHCl_3$ (^1H, 7.26 ppm) and $CDCl_3$ (^{13}C, 77.0 ppm) solvent signals. *J* values are reported in Hz. Elemental analyses were performed by Micro-Analysis, Inc. (Wilmington, DE).

General Synthesis of 1-6. $Sb(tol)_3Br_2$ (0.54 mmol) was dissolved in DCM (5 mL). A solution of the necessary diol (0.54 mmol) in DCM (2 mL) was added to the dihalostiborane solution. Et_3N (1.08 mmol) was added to the mixture. The reaction was stirred at room temperature for 1 h. The reaction was then dried under reduced pressure to yield a white solid. The product was then extracted with Et_2O (2 mL × 3). The Et_2O solution was then dried under reduced pressure to yield the crude product as a colorless oil. The oil was dissolved in MeCN (20 mL) and placed at –20 °C for 12 h. The product was collected as colorless crystals on a Hirsch funnel, washed with cold MeCN and dried under air.

Isolation of 1. Prepared with pinacol. Yield (227 mg, 82%). ^1H NMR (500 MHz, $CDCl_3$) δ=7.55 (d, ^3J= 8.0 6H; Ar-H), 7.18 (d, ^3J= 7.6, 6H; Ar-H), 2.35 (s, 9H; CH_3), 1.17 ppm (s, 12H; CH_3); $^{13}C\{^1H\}$ NMR (126 MHz, $CDCl_3$) δ=140.22, 136.95, 135.39, 129.52, 73.72, 25.85, 21.60 ppm; elemental analysis calcd (%) for $SbC_{27}H_{33}O_2$: C 63.42, H 6.51; found: C 63.15, H 6.59.

Isolation of 2. Prepared with 2*R*,3*S*-butanediol. Yield (210 mg, 81%). ^{1}H NMR (500 MHz, $CDCl_3$) δ=7.57 (d, ^{3}J= 7.9, 6H; Ar-H), 7.21 (d, ^{3}J= 7.7, 6H; Ar-H), 3.92 (dt, ^{3}J= 5.6, ^{3}J= 5.2, 2H; CH), 2.37 (s, 9H; CH_3), 1.10 ppm (d, ^{3}J= 5.7, 6H; CH_3); $^{13}C\{^{1}H\}$ NMR (126 MHz, $CDCl_3$) δ=140.50, 135.99, 135.17, 129.66, 68.61, 21.60, 18.20 ppm; elemental analysis calcd (%) for $SbC_{25}H_{29}O_2$: C 62.13, H 6.05; found: C 62.09, H 5.99.

Isolation of 3. Prepared with 1*R*,2*S*-cyclohexanediol. Yield (193 mg, 70%). ^{1}H NMR (500 MHz, $CDCl_3$) δ=7.57 (d, ^{3}J= 8.0, 6H; Ar-H), 7.21 (d, ^{3}J= 7.7, 6H; Ar-H), 3.81 (m, 2H; CH), 2.36 (s, 9H; CH_3), 1.74 (m, 2H; CH_2), 1.68 (m, 2H; CH_2), 1.55 (m, 2H; CH_2), 1.27 ppm (m, 2H; CH_2); $^{13}C\{^{1}H\}$ NMR (126 MHz, $CDCl_3$) δ=140.49, 136.09, 135.24, 129.68, 69.26, 32.29, 21.96, 21.61 ppm; elemental analysis calcd (%) for $SbC_{27}H_{31}O_2$: C 63.67, H 6.14; found: C 63.77, H 6.22.

Isolation of 4. Prepared with 2*R*,3*R*-butanediol. Yield (191 mg, 73%). ^{1}H NMR (500 MHz, $CDCl_3$) δ=7.55 (d, ^{3}J= 8.0, 6H; Ar-H), 7.20 (d, ^{3}J= 7.6, 6H; Ar-H), 3.38 (m, 2H; CH), 2.36 (s, 9H; CH_3), 1.20 ppm (d, ^{3}J= 5.6, 6H; CH_3); $^{13}C\{^{1}H\}$ NMR (126 MHz, CDCl3) δ=140.50, 136.12, 135.22, 129.66, 72.13, 21.61, 21.13 ppm; elemental analysis calcd (%) for $SbC_{25}H_{29}O_2$: C 62.13, H 6.05; found: C 62.00, H 6.21.

Isolation of 5. Prepared with 1*S*,2*S*-cyclohexanediol. Yield (198 mg, 73%). ^{1}H NMR (500 MHz, $CDCl_3$) δ=7.56 (d, ^{3}J= 8.0, 6H; Ar-H), 7.20 (d, ^{3}J= 7.7, 6H; Ar-H), 3.11 (m, 2H; CH), 2.36 (s, 9H; CH_3), 2.08 (m, 2H; CH_2), 1.70 (m, 2H; CH_2) 1.37 ppm (m, 4H; CH_2); $^{13}C\{^{1}H\}$ NMR (126

MHz, $CDCl_3$) δ=140.58, 135.94, 135.35, 129.69, 77.23, 32.79, 25.37, 21.61 ppm; elemental analysis calcd (%) for $SbC_{27}H_{31}O_2$: C 63.67, H 6.14; found: C 63.44, H 5.99.

Isolation of 6. Prepared with *S*-1,2-propanediol. Yield (200 mg, 79%). ^{1}H NMR (500 MHz, $CDCl_3$) δ=7.56 (d, ^3J= 8.0, 6H; Ar-H), 7.21 (d, ^3J= 7.7, 6H; Ar-H), 3.95 (dd, ^2J= 8.5, ^3J= 5.0, 1H; CH_2), 3.84 (dq, ^2J= 11.1, ^3J= 5.9, 1H; CH), 3.17 (dd, ^2J= 8.5, ^3J= 7.5 1H; CH_2), 2.36 (s, 9H; CH_3), 1.21 ppm (d, ^3J= 5.9, 3H; CH_3); $^{13}C\{^1H\}$ NMR (126 MHz, $CDCl_3$) δ=140.66, 135.75, 135.21, 129.73, 67.14, 65.61, 21.61, 21.47 ppm; elemental analysis calcd (%) for $SbC_{24}H_{27}O_2$: C 61.43, H 5.80; found: C 61.73, H 5.73.

X-ray crystallography. Crystals of compounds **1-6** were grown as described above, crystals of $Sb(tol)_3$ were grown from a saturated EtOH solution at –20 °C over 12 h, and crystals of the decomposition product were grown from a saturated MeCN solution at –20 °C over 12 h. X-ray diffraction quality crystals of each were selected under a microscope, loaded onto a nylon fiber loop using Paratone-*n*, and mounted onto a Rigaku XtaLAB Synergy-S single crystal diffractometer. Each crystal was cooled to 100 K under a stream of nitrogen. Diffraction of Cu Kα radiation from a PhotonJet-S microfocus source was detected using a HyPix-6000HE hybrid photon counting detector. Screening, indexing, data collection, and data processing were performed with CrysAlisPro. The structures were solved using SHELXT and refined using SHELXL.[24, 25] All non-H atoms were refined anisotropically. H atoms were placed at geometrically calculated positions and refined with a riding model. The U_{iso} of the H atoms were set equal to 1.2(U_{eq}) of the C atom to which each is attached for CH_2 and aromatic CH units or 1.5(U_{eq}) for methyl groups.

Acknowledgements

The single-crystal X-ray diffractometer housed in the UCSC X-ray Diffraction Facility was funded by NSF MRI grant 2018501 and this work was further supported by a Hellman Fellowship to T.C.J.

Conflicts of interest

There are no conflicts to declare.

Author contributions

B.L.-K. performed experiments, and B.L.-K. and T.C.J. wrote the manuscript.

Data availability statement

Crystallographic data for $Sb(tol)_3$, **1**-**6**, and the decomposition product described in the ESI have been deposited at the Cambridge Crystallographic Data Centre, under deposition numbers CCDC 2265793-2265800, and can be obtained from https://www.ccdc.cam.ac.uk/structures/. Full NMR spectra and thermal ellipsoid plots not provided in the main text are available in the ESI PDF document.

References

1. F. Frézard, C. Demicheli and R. R. Ribeiro, *Molecules*, 2009, **14**, 2317-2336.
2. J. Duffin and P. René, *J. Hist. Med. Allied Sci.*, 1991, **46**, 440-456.
3. A. W. Diamond, V. C. Fayad and P. S. McKinley, *J. Field Ornithol.*, 2007, **78**, 436-439.
4. R. E. Tapscott, R. L. Belford and I. C. Paul, *Coord. Chem. Rev.*, 1969, **4**, 323-359.
5. B. R. Do Prado, A. Islam, F. Frézard and C. Demicheli, in *Drug Discovery for Leishmaniasis*, 2017, DOI: 10.1039/9781788010177-00199, ch. 10, pp. 199-223.

6. World Health Organization, *Leishmaniasis* [Fact sheet], https://www.who.int/news-room/fact-sheets/detail/leishmaniasis, (accessed 2023/05/26).
7. P. D. Marsden, *Rev. Soc. Bras. Med. Trop.*, 1985, **18**, 187-198.
8. F. Frézard, P. S. Martins, M. C. M. Barbosa, A. M. C. Pimenta, W. A. Ferreira, J. E. de Melo, J. B. Mangrum and C. Demicheli, *J. Inorg. Biochem.*, 2008, **102**, 656-665.
9. B. Gyurcsik and L. Nagy, *Coord. Chem. Rev.*, 2000, **203**, 81-149.
10. B. Lindquist-Kleissler, M. Weng, P. Le Magueres, G. N. George and T. C. Johnstone, *Inorg. Chem.*, 2021, **60**, 8566-8574.
11. H. Barucki, S. J. Coles, J. F. Costello and M. B. Hursthouse, *J. Organomet. Chem.*, 2001, **622**, 265-273.
12. Y. Matsumura, M. Shindo and R. Okawara, *J. Organomet. Chem.*, 1971, **27**, 357-363.
13. C. V. Stevani and W. J. Baader, *J. Chem. Res.*, 2002, **2002**, 430-432.
14. A. L. Baumstark, M. E. Landis and P. J. Brooks, *J. Org. Chem.*, 1979, **44**, 4251-4253.
15. V. V. Sharutin, O. K. Sharutina and N. A. Shalabanova, *Russ. J. Coord. Chem.*, 2019, **44**, 765-771.
16. R. R. Holmes, R. O. Day, V. Chandrasekhar and J. M. Holmes, *Inorg. Chem.*, 1987, **26**, 163-168.
17. A. I. Poddel'sky, G. K. Fukin and E. V. Baranov, *Russ. J. Coord. Chem.*, 2022, **48**, 902-908.
18. A. W. Addison, T. N. Rao, J. Reedijk, J. van Rijn and G. C. Verschoor, *J. Chem. Soc. Dalton Trans.*, 1984, 1349-1356.
19. E. L. Muetterties, W. Mahler and R. Schmutzler, *Inorg. Chem.*, 1963, **2**, 613-618.
20. E. L. Muetterties, W. Mahler, K. J. Packer and R. Schmutzler, *Inorg. Chem.*, 1964, **3**, 1298-1303.
21. C. Brabant, J. Hubert and A. L. Beauchamp, *Can. J. Chem.*, 1973, **51**, 2952-2957.
22. K.-W. Shen, W. E. McEwen, S. J. La Placa, W. C. Hamilton and A. P. Wolf, *J. Am. Chem. Soc.*, 1968, **90**, 1718-1723.
23. G. M. Sheldrick, *Acta Crystallogr., Sect. A: Found. Adv.*, 2015, **71**, 3-8.
24. G. M. Sheldrick, *Acta crystallogr., Sect. C: Struct. Chem.*, 2015, **71**, 3-8.